JOURNAL OF MATERIALS SCIENCE 23 (198) 4547-4553

# Effect of non-stoichiometry on the sintering of doped $TiO_2$

P. ODIER
*Centre de Recherches sur la Physique des Hautes Températures, CNRS, 45071 Orleans Cedex 2, France*

J. LECOMTE, J. P. LOUP
*Laboratoire de Physique Electronique et Thermodynamique des Oxydes, UFR des Sciences et Techniques, Parc de Grandmont, 37200 Tours, France*

The sintering of $TiO_2$ has been studied with respect to oxygen partial pressure ($P_{O_2}$) and doping content. From the microstructural evolution, it is obvious that a decrease of the oxygen pressure promotes the densification with a comparatively smaller grain growth than in air sintering. This fact has been related with the influence of defects on the sintering. Both effects of $P_{O_2}$ and tantalum doping have been studied. They are interpreted on the basis of a model involving interstitial titanium, electron holes, titanium vacancies and complexes associating titanium vacancies with tantalum substituted titanium. This latter complex is probable according to previous microscopic studies of defects in $TiO_{2-x}$ and may be important in highly doped compounds. The formation of such associates reduces the mobile defect concentration, however a decrease of the $P_{O_2}$ favour their dissociation. The titanium vacancies which are thus released allow the titanium ions to migrate, a necessary condition for the sintering.

## 1. Introduction

Sintering is a phenomenon controlled by a transport of matter, it is thus expected to be affected by non-stoichiometric defects. Many studies have been made on the non-stoichiometry of $TiO_2$ as well as on sintering but very few attempted to look at their mutual influence. This paper gives some experimental results in this area.

Non-stoichiometry can be obtained in two ways: (i) by changing the oxygen potential in equilibrium with the oxide; (ii) by doping the compound with aliovalent cations such as $Nb^{5+}$ or $Ta^{5+}$. In the present paper both effects have been investigated on similar batches of powder.

Two aspects of the oxygen partial pressure effect have been considered. Firstly, how does the microstructure and density of a sample change during its sintering if the $P_{O_2}$ decreased suddenly? and secondly is it possible to interpret, at least qualitatively, the modifications on the shrinkage induced by a decrease of $P_{O_2}$ during an isothermal sintering?

In a third and complementary experiment, the affect of doping by tantalum on the sintering at various oxygen pressures has been studied.

Finally the results are discussed on the basis of the defect theory in which point and complex defects are taken into account and emphasize the role of titanium vacancies on the sintering.

## 2. Experimental procedure

### 2.1. Powder preparation

Gels of niobium-doped titania ($Nb/Ti = 1.2 \times 10^{-3}$) were obtained from Thann and Mulhouse and prepared in the form of ceramic powder. They were redispersed in aqueous solution with an ultraturax, then spray dried (Büschi spraydrier), calcined at 600° C in air and compacted isostatically (480 MPa) in the shape of cylinders for sintering. The powder comprises small crystallites of 60 nm, they are aggregated in spheroidal compacts of 0.3–0.5 $\mu$m (Fig. 1). The aggregates are themselves agglomerated in 1–2 $\mu$m compacts which are almost totally flattened out by the compaction as shown by the pore size distribution measured by mercury porosimetry, Fig. 1. The influence of the pH on the process has been tested: if the pH has an effect on the agglomeration, it is not so pronounced on the sinterability, the agglomerates being rather soft in that particular case. This batch will be called batch 1 in the following.

Batch 2 of tantalum-doped $TiO_2$ was prepared by simultaneous hydrolysis of titanium isopropoxyde and tantalum ethoxyde. The sol was filtered, calcined at 400° C for crystallization of the anatase phase and annealed at 630° C under reducing conditions (30% CO–70% $CO_2$). This low $P_{O_2}$ treatment promotes the tantalum incorporation according to the reaction

$$Ta_2O_5 \rightarrow 2Ta_{Ti}^{\cdot} + 2e + 4O_O^{x} + \tfrac{1}{2} O_2 \qquad (1)$$

The samples were then deagglomerated and isostatically compacted at 400 MPa.

The internal porosity has been measured by an automatic mercury porosimeter (Coulter A 9300) and the microstructure obtained by SEM (Jeol 100 CX). The sintering was done in isothermal conditions under

0022-2461/88 $03.00 + .12 

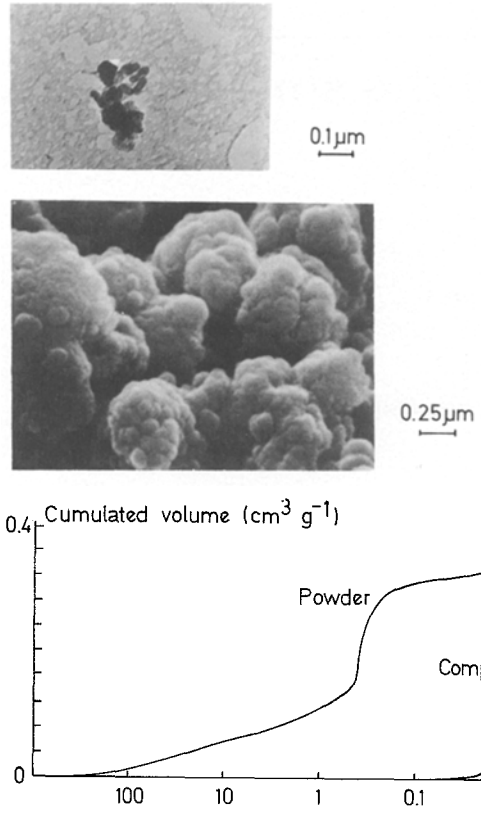


*Figure 1* Texture of niobium doped $TiO_2$ by TEM, SEM and mercury porosimetry. [Nb]/[Ti] = $1.2 \times 10^{-3}$.

various $P_{O_2}$ ($Ar$–$O_2$, $CO$–$CO_2$). The shrinkage was measured at the plateau by using a differential dilatometer under controlled $P_{O_2}$ (Adhamel) with a dense polycrystalline titania as a reference. This procedure enables us to extract the exact contribution induced on sintering by a change of the $P_{O_2}$ at constant temperature. In the following we report $\Delta l/L_p(\%)$ as a function of $P_{O_2}$, $L_p$ being the length of the sample at the beginning of the plateau. Heating was carried out at a constant rate of $5°C\,mm^{-1}$ in air and the $P_{O_2}$ modified after reaching the plateau.

## 3. Results

### 3.1. Effect of the oxygen pressure and time on the microstructure evolution

Several samples of batch 1 were sintered in air at 1100° C. The evolution of their microstructure (on fractured surfaces) is shown in Fig. 2, together with their porosity distribution.

Notice first the poor densification achieved at the early stage of sintering at 1100° C. The density reaches 77% of the theoretical density ($d_{th}$) corresponding to a shrinkage of 14% according to $d/d_{th} = d_0/d_{th}(1 - \Delta l/l_0)^{-3}$ where $d$, $d_0$, $d_{th}$ are the final, and initial density and $\Delta l/l_0$ the relative shrinkage (%); the green compaction $d_0$ was in the range of 50%. Most of the porosity is open at this stage of the sintering. It is interesting to compare the actual microstructure of this ceramic to that obtained by Barringer *et al.*

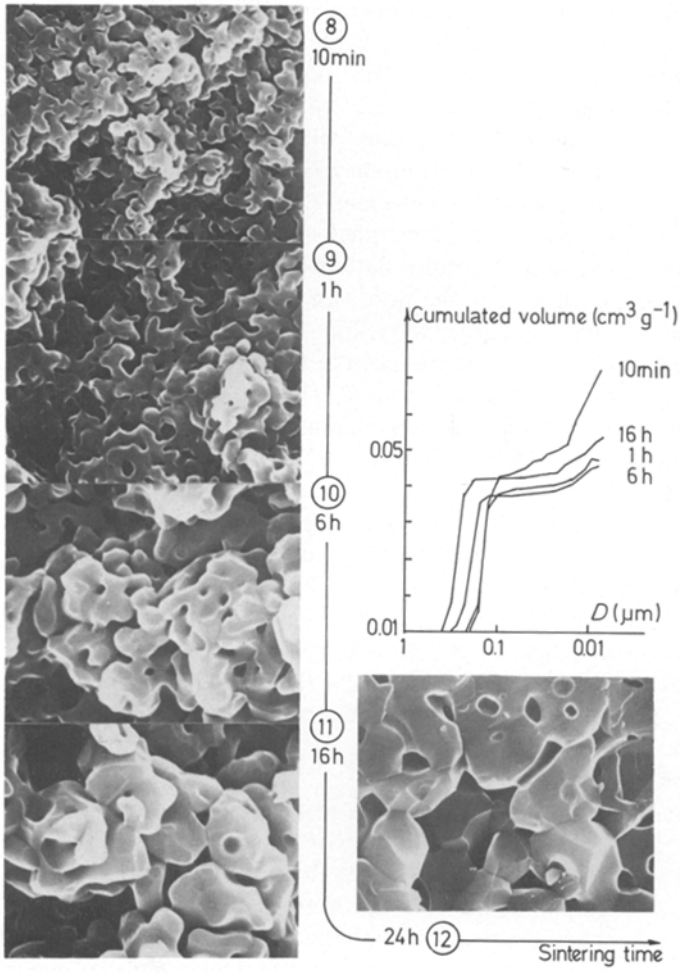


*Figure 2* Evolution of microstructure of $TiO_2$ (Batch 1) during air sintering at 1100° C. [Nb]/[Ti] = $1.2 \times 10^{-3}$, heating rate = $300°C\,h^{-1}$.

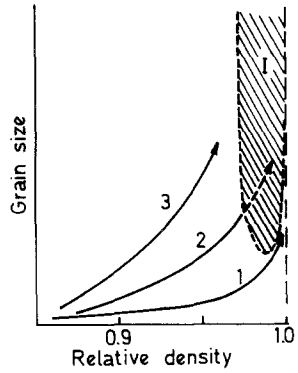


*Figure 3* Schematic grain growth–density map.

[1] from monodispersed powders, synthesized by controlled hydrolysis of alkoxides. If the overall texture is rather similar (see Figs 5 and 6 of [1]), it is, however, clear that the grain size 1 $\mu$m is larger in our case (3 times approximately), the main textural difference being a much more agglomerated structure. Note that the agglomerates contain quasi-isolated pores that are certainly open. The grain growth with time is considerable in our case, the grain size being multiplied by a factor of 5 while they become faceted after 16 h of treatment. This faceting occurs only after 1 h for monosized powders without any perceptible grain growth [1].

Fig. 2 also shows the evolution of the open porosity as measured by mercury porosimetry. It is obvious that the densification is very small while open pores increase in size (0.15 to 0.5 $\mu$m after 16 h). From the microstructure and the porosimetry, one can conclude that the round quasi-isolated pores are transferred to the outside of the grains and collapse with the porous volume.

The evolution of sintering can be comparatively described with the help of grain growth–density maps [1–4]. According to Barringer *et al.* [1] practically no grain growth should occur for a mono-sized compact until 90% of density, Fig. 3, while for an agglomerated powder the grain growth occurs simultaneously to densification. It is the case of our sample which follows a typical path 2 while mono-sized particle would follow a path 1.

The sintering in a low $P_{O_2}$ of $8 \times 10^{-6}$ Pa (under $CO/CO_2$ mixture) behaves quite differently. Heating to 1100° C was done under air (at a rate of 5° C min$^{-1}$ as previously) and the low $P_{O_2}$ applied after 1 h at the plateau. The microstructure evolution as well as the porosity change are shown in Fig. 4. Obviously an important enhancement of the densification is obtained, without grain growth, during the early stage of the treatment. Upon extending the dwell time, a rapid grain growth occurs with even a de-densification. It is suggested that after an optimal density, the partial reduction of the sample by the low $P_{O_2}$ creates additional porosity. In fact the fractured samples were generally grey or dark blue inside indicating extensive non-stoichiometry. With optimized conditions the beneficial effect of the low $P_{O_2}$ treatment is thus twofold: (i) rapid elimination of the quasi-isolated porosity, (ii) enhanced densification with a delated grain growth in comparison to the air sintering. The sintering follows path 3 in Fig. 3. The sintering acceleration mechanism will be further commented on in the next section.

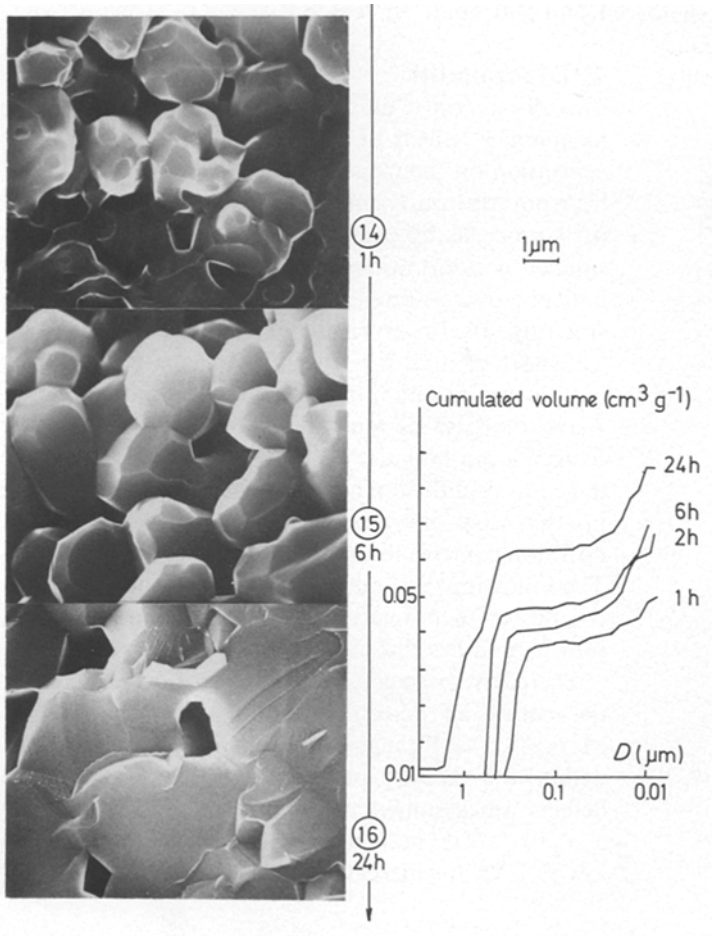


*Figure 4* Evolution of the microstructure of $TiO_2$ (Batch 1) during sintering under a low $P_{O_2}$ ($8 \times 10^{-6}$ Pa) at 1100° C. [NB]/[Ti] = $1.2 \times 10^{-3}$, heating rate = 300° C h$^{-1}$.

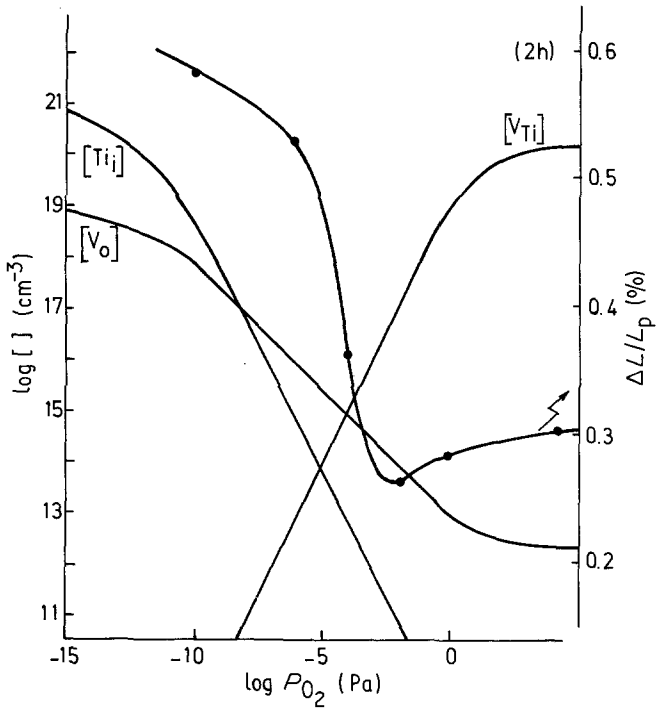


*Figure 5* Relative shrinkage plotted against $P_{O_2}$ for tantalum-doped $TiO_2$ at 1100° C. The relative shrinkage refers to the length of the sample at the beginning of the plateau. [Ta]/[Ti] = $2 \times 10^{-2}$.

### 3.2. Influence of the dopant concentration and $P_{O_2}$ on the shrinkage rate

In a subsequent experiment the evolution of the shrinkage with the $P_{O_2}$ was investigated with a tantalum-doped material (Batch 2) containing $2 \times 10^{-2}$ atomic fraction of tantalum. The relative variation of the sample length (with respect to the length at the beginning of the isothermal treatment) is reported for a constant temperature of 1100° C in Fig. 5. The low $P_{O_2}$ is applied after the temperature has been stabilized. The shrinkage rate at the plateau is quite small and the recorded variation represents the macroscopic effect of the $P_{O_2}$ on the sintering. While small for oxygen partial pressure up to $P_{O_2} \sim 10^{-3}$ Pa, the length reduction is notably accelerated below this pressure. Similar results were obtained for batch 1.

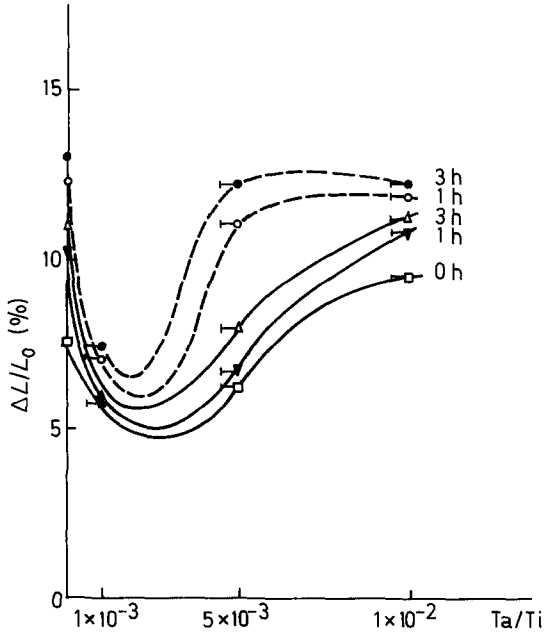


*Figure 6* Evolution of the sintering of tantalum-doped $TiO_2$ plotted against tantalum content for $P_{O_2} = 2 \times 10^{-10}$ Pa (----) and $P_{O_2} = 2 \times 10^{4}$ Pa (——) at 1100° C.

Finally the shrinkage of tantalum-doped $TiO_2$ has been measured as a function of the dopant concentration and for two oxygen partial pressures, is reported in Fig. 6. The variation in the shrinkage cannot be attributed to variations in the green density that was approximately constant in that series ($\sim 55\%$ $d_{th}$), it is, therefore, attributed to an intrinsic evolution with the tantalum content. Note that the dopant concentration of the "pure" sample has been determined by analysing the conductivity data as a function of $P_{O_2}$ [5] by using the same procedure as ref. [6] and represents approximately 200 p.p.m. in acceptor states for batch 1 and 500 p.p.m. for batch 2.

## 4. Discussion

This discussion is an attempt to explain the phenomenological effects of changing $P_{O_2}$ and doping concentration on the densification kinetic of $TiO_2$. Mass transport obviously controls the densification rate and (if it proceeds by charged ions) the species with the smaller concentration times mobility product will limit the overall rate [7]. In the intermediate stage of sintering, Barringer *et al.* [1] have shown that bulk transport of matter is the principal path; obviously oxygen and titanium ions must move simultaneously. As in the case of alumina [8] we suppose that the oxygen grain boundary diffusion is fast and therefore the cationic diffusion is the rate limiting step. We take up this view point and suppose the titanium bulk diffusion controls the kinetics of the sintering of $TiO_2$. The following discussion is focussed on point defects, it assesses their relationship with $P_{O_2}$ and discusses how it modifies the sinterability.

There have been considerable discussions concerning the nature of defects in non-stoichiometric $TiO_2$. Marucco *et al.* [9] suggest that there are three domains within the $TiO_{2-x}$ phase where the predominant defects are assumed to be: $TiO_2$–$Ti_nO_{2n-1}$ for $x \gtrsim 5 \times 10^{-3}$, $Ti^{4\cdot}$ at high temperature ($\sim 900°$ C) and low $P_{O_2}$, $V_O^{2\cdot}$ for increasing $P_{O_2}$ but prevailing at lower

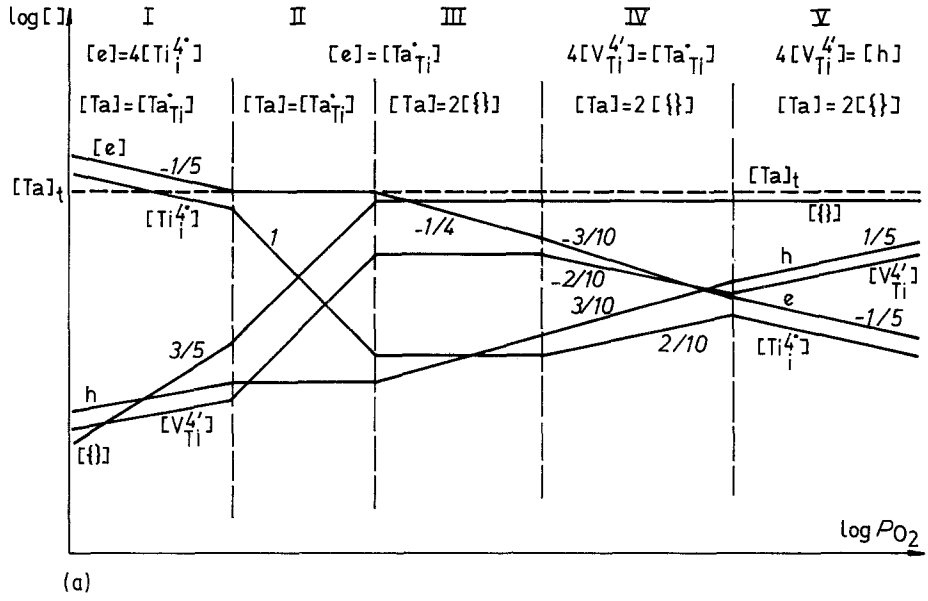


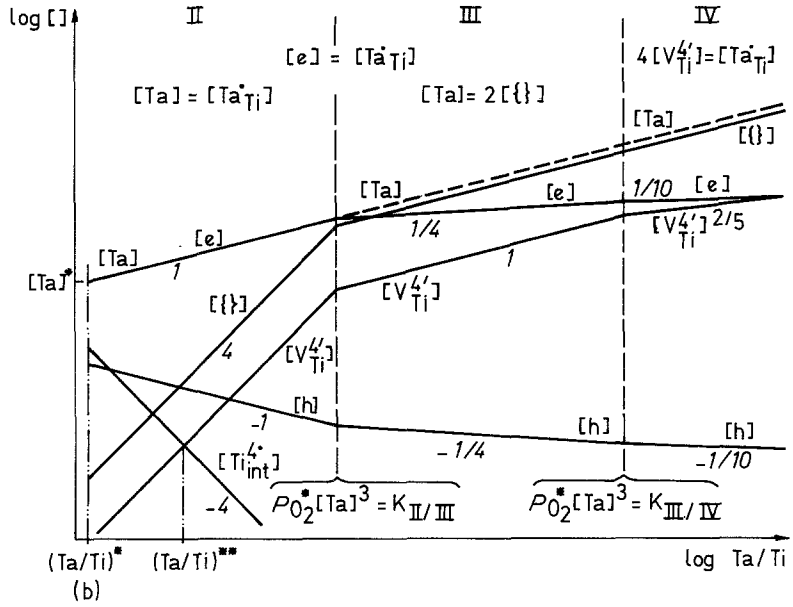


*Figure 7* (a) Defect concentration plotted against $P_{O_2}$ and tantalum concentration for tantalum-doped $TiO_2$. The evolution of the associate $\{V_{Ti}^{2'}, 2Ta_{Ti}^{\cdot}\}^x$ is indicated. (b) Defect concentration versus Ta concentration for Ta doped $TiO_2$.

temperature. Further studies by electron microscopy have revealed (on cooling) the formation of clusters [10] prefiguring the crystallographic shear planes (CSP) and planar defects. These clusters consist of linear arrangements along [1 0 0] or [0 1 0] containing two-faced shared octahedral pairs bounded by a titanium vacancy. In this linear interstitial model two $Ti^{3+}$ occupy octahedral interstices and two $Ti^{3+}$ substitute one $Ti^{4+}$ cation in normal sites; their aggregation lead to the CSP. This can be also considered as a complex defect associating two interstitial titanium, one cationic vacancy and two electrons trapped on two titanium sites, this complex is neutral. For slightly sub-stoichiometric oxides (either by reduction or low valency cation doping) the same type of model account for the presence of oxygen vacancies [11, 12] associated with $2Cr^{3+}$ in face-shearing octahedron sites. In the following we have calculated the variation of point defects $Ti_i^{4\cdot}$, $V_O^{2\cdot}$, $V_{Ti}^{4'}$ with $P_{O_2}$ and $Ta_{Ti}$ concentration, Fig. 7 and Table I. In addition we have considered the complex associate, bonding $V_{Ti}^{2'}$ (a titanium vacancy with two trapped holes) with two tantalum on titanium sites

$$V_{Ti}^{4'} + 2Ta_{Ti}^{\cdot} + 2h = \{V_{Ti}^{2'}, 2Ta_{Ti}^{\cdot}\}^x$$

$$k_a = \frac{[\{\ \}]}{[V_{Ti}^{4'}][Ta_{Ti}^{\cdot}]^2[h]^2}$$

This type of association is very consistent with the cluster precursor described above (Bursill *et al.* [10–12]) and is in agreement with electrical properties of (Ti, Ta)$O_2$ or (Ti, Nb)$O_2$ solid solutions [13, 14]. Furthermore, it explains well some features of electrical

TABLE I Defect equilibrium

(1) $O_2(g) = V_{Ti}^{4'} + 4h + 2O_O^x$, $k_3 = \dfrac{[V_{Ti}^{4'}][h]^4}{P_{O_2}}$

(2) $Ti_{Ti}^x + 2O_O^x/Ti_i^{4\cdot} + 4e + O_2(g)$, $k_{11} = [Ti_i^{4\cdot}][e]^4 P_{O_2}$

(3) $O = e + h$ $k_4 = [e][h]$

(4) $V_{Ti}^{4'} + 2Ta_{Ti}^{\cdot} + 2h = \{V_{Ti}^{2'}, 2Ta_{Ti}^{\cdot}\}^x$, $k_a = \dfrac{[\{\ \}]}{[V_{Ti}^{4'}][Ta_{Ti}^{\cdot}]^2[h]^2}$

(5) Electroneutrality condition

$4[V_{Ti}^{4'}] + [e] = 4[Ti_i^{4\cdot}] + [Ta_{Ti}^{\cdot}] + [h]$

(6) Tantalum conservation

$[Ta] = [Ta^x] + 2[\{\ \}] + [Ta_{Ti}^{\cdot}]$

[ ] denotes concentrations

[{ }] denotes concentrations of $\{V_{Ti}^{2'}, 2Ta_{Ti}^{\cdot}\}^x$

TABLE II Defect concentration

| | I | II | III | IV | V |
|---|---|---|---|---|---|
| $K_a K_4^2 > 1$ | $[e] = 4[Ti_i^{4\cdot}]$<br>$[Ta] = [Ta_{Ti}^{\cdot}]$ | $[e] = [Ta_{Ti}^{\cdot}]$<br>$[Ta] = [Ta_{Ti}^{\cdot}]$ | $[e] = [Ta_{Ti}^{\cdot}]$<br>$[Ta] = 2[\{\quad\}^x]$ | $4[V_{Ti}^{4'}] = [Ta_{Ti}^{\cdot}]$<br>$[Ta] = 2[\{\quad\}^x]$ | $4[V_{Ti}^{4'}] = [h]$<br>$[Ta] = 2[\{\quad\}^x]$ |
| $[Ta_{Ti}^{\cdot}]$ | $[Ta]$ | $[Ta]$ | $\frac{K_4^{1/2}}{(2K_3)^{1/4}}\left(\frac{[Ta]}{K_a}\right)^{1/4} P_{O_2}^{-1/4}$ | $\frac{1}{K_3^{1/5}}\left(\frac{[Ta]}{K_a}\right)^{2/5} P_{O_2}^{-1/5}$ | $\frac{1}{2^{1/10}K_3^{3/10}}\left(\frac{[Ta]}{K_a}\right)^{1/2} P_{O_2}^{-3/10}$ |
| $[e]$ | $(4K_{11})^{1/5} P_{O_2}^{-1/5}$ | $[Ta]$ | $\frac{K_4^{1/2}}{(2K_3)^{1/4}}\left(\frac{[Ta]}{K_a}\right)^{1/4} P_{O_2}^{-1/4}$ | $\frac{K_4}{2^{1/2}K_3^{3/10}}\left(\frac{[Ta]}{K_a}\right)^{1/10} P_{O_2}^{-3/10}$ | $\frac{K_4}{(4K_3)^{1/5}} P_{O_2}^{-1/5}$ |
| $[h]$ | $\frac{K_4}{(4K_{11})^{1/5}} P_{O_2}^{+1/5}$ | $K_4[Ta]^{-1}$ | $(2K_3)^{1/4}(K_4^2 K_a)^{1/4}\left(\frac{P_{O_2}}{[Ta]}\right)^{1/4}$ | $2^{1/2}K_3^{3/10}\left(\frac{K_a}{[Ta]}\right)^{1/10} P_{O_2}^{3/10}$ | $(4K_3)^{1/5} P_{O_2}^{1/5}$ |
| $[V_{Ti}^{4'}]$ | $\frac{K_3(4K_{11})^{4/5}}{K_4^4} P_{O_2}^{1/5}$ | $\frac{K_3}{K_4^4}[Ta]^4 P_{O_2}$ | $\frac{1}{2K_4^2}\frac{[Ta]}{K_a}$ | $\frac{1}{4K_3^{1/5}}\left(\frac{[Ta]}{K_a}\right)^{2/5} P_{O_2}^{-1/5}$ | $\frac{K_3^{1/5}}{4^{4/5}} P_{O_2}^{1/5}$ |
| $[Ti_i^{4\cdot}]$ | $\frac{(4K_{11})^{1/5}}{4} P_{O_2}^{-1/5}$ | $K_{11}[Ta]^{-4} P_{O_2}^{-1}$ | $\frac{2K_{11}K_3}{K_4^2}\frac{K_a}{[Ta]}$ | $\frac{4K_3^{6/5}K_{11}}{K_4^4}\left(\frac{K_a}{[Ta]}\right)^{2/5} P_{O_2}^{+1/5}$ | $\frac{K_{11}(4K_3)^{4/5}}{K_4^4} P_{O_2}^{-1/5}$ |
| $[\{\quad\}]$ | $\frac{K_3(4K_{11})^{2/5}}{K_4^2} K_a[Ta]^2 P_{O_2}^{3/5}$ | $\frac{K_3}{K_4^2} K_a[Ta]^4 P_{O_2}$ | $\frac{[Ta]}{2}$ | $\frac{[Ta]}{2}$ | $\frac{[Ta]}{2}$ |
| $\frac{[\{\quad\}]}{[V_{Ti}^{4'}]}$ | $\frac{K_4^2}{(4K_{11})^{2/5}} K_a[Ta]^2 P_{O_2}^{2/5}$ | $K_4^2 K_a$ | $K_4^2 K_a$ | $2K_3^{1/5} K_a^{2/5}[Ta]^{3/5} P_{O_2}^{1/5}$ | $\frac{2^{3/5}}{K_3^{1/5}}[Ta] P_{O_2}^{-1/5}$ |
| | $P_{O_2}[Ta]^5 = 4K_{11}$ | $P_{O_2}[Ta]^3 = \frac{K_4^2}{2K_3K_a}$ | $P_{O_2}[Ta]^3 = \frac{K_4^{10}K_a^3}{2^5K_3}$ | $[Ta]\,P_{O_2}^{-1} = 2K_3K_a$ | |

data at high temperature obtained several years ago by Baumard *et al.* [15, 16] for tantalum- or niobium-doped rutile. In these samples, there is a significant departure from the ideal behaviour of the electron carrier concentration ($e$) with the doping content $D$ (Nb, Ta) in the high oxygen pressure range. The dependence appears to be slower than excepted in the ideal case. Defect association such as that proposed here would give a much slower dependence: $e \propto D^{1/10}$ instead of $e \propto D^{1/4}$ in the point defect model and thus could provide a satisfactory model.

Returning to the sintering, one must explain the variation in Figs 5 and 6. Let us consider Fig. 5 first. Referring to range II of Fig. 7, one see that $[Ti_i]$ decreases with increasing $P_{O_2}$ thus reducing the densification rate until the titanium vacancy concentration becomes significant. Indeed a small rise of the densification is observed above $10^{-2}$ Pa but not to the extent expected if no associations were present. In fact, when $P_{O_2}$ is increased, the $V_{Ti}^{4'}$ creation is limited by associate formation, the maximum of which is $[Ta]/2k_a k_4^2$ (Table II) instead of $1/4[Ta]$ in a free defect model ($k_4 = [e][h]$, see range III in Fig. 7). To investigate creep, Philpot *et al.* [17] considered a steady creep limited by the oxygen lattice diffusion and used a free defect model. However, the observed variations of the strain rate with $P_{O_2}$ and/or tantalum content is much smaller than theoretically predicted. A model with defect association would provide a better explanation.

Fig. 6 shows a significant decrease of the sintering rate below [Ta] = 0.2%. This is in agreement with earlier experiments [18] and with the free defect model. It qualitatively follows that the variations of log $([Ti_i^{4'}] + [V_{Ti}^{4'}])$ with log [Ta]/[Ti] when $[Ta]/[Ti] \ll (Ta/Ti)^{**}$ as defined in Fig. 7b. On the other hand, decreasing the oxygen partial pressure from $2 \times 10^4$ to $2 \times 10^{-10}$ Pa increases the shrinkage (Fig. 6) that is obviously predicted by the defect theory for small doping rate (Fig. 7a) because in this range interstitial titanium is the dominant defect and its concentration rises when $P_{O_2}$ decreases. For higher doping rates, associations such as $\{V_{Ti}^{2'}, 2Ta_{Ti}^{2\cdot}\}^x$ become large, Fig. 7b, and increase simultaneously as $[V_{Ti}^{4'}]$ with the tantalum content. However associations are not expected to be useful in sintering due to their low mobility. Under a low $P_{O_2}$ treatment they probably dissociate with a consecutive migration of the $V_{Ti}^{4'}$ toward the surface. This process may render possible the titanium transport needed in the sintering.

The following mechanism is therefore proposed to explain the relationship between oxygen pressure and sinterability in doped $TiO_2$:

(i) Upon an oxygen pressure reduction at the beginning of the sintering plateau, the hole concentration decreases and favour the dissociation of the associates: Equation 4 in Table I;

(ii) Titanium vacancies are released which allow titanium ions to migrate and therefore to promote the sintering.

## 5. Conclusion

The discussion, so far, explains most of the observed effects of non-stoichiometry on the sintering of $TiO_2$. It is clearly proved that defects promote bulk diffusion and therefore help the sintering. However, if an increase in the defect concentration accelerates the kinetic, it will not increase the driving force for sintering, on the contrary it lowers the free enthalpy of the system. Accordingly after the system has reached its "end-point" as in Fig. 3, the re-crystallization with grain growth occurs as observed in the first experiments reported in Fig. 2. For rather high doping levels $\sim 2 \times 10^{-2}$, associations are expected to occur, reducing the mobile defect concentration. By reducing the $P_{O_2}$ one can dissociate the complex, release titanium vacancies and therefore promote the sintering.

## References


1. E. A. BARRINGER, R. J. BROOK and H. K. BOWEN, in "Sintering and Heterogeneous Catalysis", *Mat. Sci. Res.* Vol. 16, edited by G. C. Kuczynoski, A. E. Miller and G. A. Sargen (Plenum Press, New York, 1983) pp. 1–21.
2. M. P. HARMER, *Adv. Ceram.* **10** (1984) 679.
3. R. J. BROOK, in "Ceramics Today and Tomorrow", edited by Shigehaur, Naka, Noohiro Soga and Stoichikume (The Ceramic Society, Japan, 1986) pp. 87–100.
4. M. F. YAN, *Mater. Sci. Engng* **48** (1981) 53–72.
5. J. LECOMTE, unpublished results.
6. J. F. BAUMARD, D. PANIS and D. RUFFIER, *Rev. Int. Htes Temp. Refract.* **12** (1975) 321.
7. R. S. GORDON, *J. Amer. Ceram. Soc.* **56** (1973) 147.
8. F. A. KROGER, *ibid.* **12** (1984) 390.
9. J. F. MARUCCO, J. GAUTRON and P. LEMASSON, *J. Phys. Chem. Solids* **42** (1981) 363.
10. L. A. BURSILL and M. G. BLANCHIN, *J. Phys. Lett.* **44** (1983) 2165.
11. *Idem., J. Solid State Chem.* **51** (1984) 321.
12. L. A. BURSILL, D. J. SMITH and PENG JU LIN, *ibid.* **56** (1985) 203.
13. B. POUMMELEC and J. F. MARUCCO, *J. Phys. Chem. Solids* **46** (1985) 71.
14. C. SCHLENKER, S. AHMED, R. BUDER and M. GOURMALA, *J. Phys. C* **12** (1979) 3503.
15. J. F. BAUMARD and E. TANI, *J. Chem. Phys.* **67** (1977) 857.
16. E. TANI and J. F. BAUMARD, *J. Solid State Chem.* **32** (1980) 105.
17. K. PHILPOT, *J. Mater. Sci.* **18** (1983) 1698.
18. G. R. MILLER and O. W. JOHNSON, "Material Science Research", Vol. 11, edited by H. Palmour III, R. E. Davis and T. M. Hare (Plenum Press, New York, 1978) p. 181.



*Received 7 December 1987*
*and accepted 29 April 1988*